

Optimal Velocity Model Based CACC Controller for Urban Scenarios

Anas Abulehia, Reza Dariani^a and Julian Schindler^b

Institute of Transportation Systems, German Aerospace Center (DLR), Braunschweig, Germany

Keywords: CCAC, Optimal Velocity Model, Linear Quadratic Controller.

Abstract: To address the current high level of congestion, a connected vehicle system in the form of a platoon or Cooperative Adaptive Cruise Control (CACC) presents a promising solution. This system significantly reduces stop-and-go traffic, as well as fuel consumption. A Cooperative Adaptive Cruise Control (CACC) system comprises two or more closely-following vehicles traveling at a desired cruising velocity and distance headway. Compared with human drivers, such a system has the advantage of reducing inter-vehicle distance, making it a promising solution for mitigating traffic congestion as well as reducing aerodynamic drag, and fuel consumption. This work aims to introduce a new Cooperative Adaptive Cruise Control (CACC) based on the optimal velocity model in traffic dynamics. Several controllers for the introduced CACC system will be presented, particularly various versions of the linear quadratic controller. Simulation scenarios for these controllers will also be discussed.

1 INTRODUCTION

Mobility is indispensable in human life, impacting various aspects from daily commutes to exploring distant tourist destinations. It is an integral part of our existence. Globally, in 2012, the average distance traveled per person was 7,000 miles annually. Over 80% of this travel occurred in vehicles, including cars, taxis, buses, and similar modes of transportation (Brand et al., 2019).


Tackling traffic jams is challenging because, in many cases, no clear reason for the emergence of new congestion is found. A false braking incident somewhere could be propagated and transformed into a traffic jam. A driving assistance system like Cooperative Adaptive Cruise Control (CACC) offers a solution to the traffic problem. The main advantage of CACC is improving traffic flow and reducing traffic congestion. Other benefits include enhanced safety and comfort when compared with other vehicular systems. According to (Shladover et al., 2015), the time gap can be reduced from about 1.4 to 0.6 seconds when using CACC.


The CACC concept is the combination of automated speed control with a cooperative element, such as Vehicle-to-Vehicle (V2V) and/or Infrastructure-to-Vehicle (I2V) communication (Shladover et al.,

2015). The literature of CACC system is well established in the scientific community. In (Wang et al.,) a review on CACC system was presented. Framing our work within it, the flow of information is considered a vehicle parameter, allowing for various possible information flow topologies. Although the simulation section focuses on three specific topologies, it's important to note that bidirectional information flow is not defined; the system permits information to go downstream only. The control problem has been addressed individually for each vehicle without employing any centralization concept.

In addressing challenges, recent works such as those (Hsueh et al., 2022), (Bekiaris-Liberis, 2023), (Xing et al., 2022), (Fu et al., 2023) have been dedicated to mitigating the impact of time delay, which can adversely affect the performance of any baseline CACC. Furthermore, there is a growing emphasis on enhancing the robustness and security of the system against communication degradations or attacks. (Liu et al., 2023), (Yang et al., 2023), and (Zhongwei et al.,) have contributed significantly to this area, reflecting the maturation of CACC technology.

This paper focuses on the V2V CACC system. The first section of this paper discusses the CACC system using the Optimal Velocity Model, and the MOTIF concept is introduced. Central Optimal Control has been addressed by (Ge and Orosz, 2016). The second section deals with the control problem at the

^a  <https://orcid.org/0000-0002-1091-8793>

^b  <https://orcid.org/0000-0001-5398-8217>

vehicle level (decentralized). The Linear Quadratic Regulator was utilized with different variations. The third section shows closed-loop simulations of different scenarios.

2 OPTIMAL VELOCITY MODEL

The Optimal Velocity model (Bando et al., 1994), (Bando et al., 1995), is a single-lane mathematical traffic model. It models traffic using physically meaningful parameters. The model describes traffic congestion by analyzing the behavior of each individual vehicle, utilizing the headway between preceding and following vehicles to compute the following vehicle's velocity. The model has garnered significant scientific attention due to its stability in both analytical and numerical analyses. The Optimal Velocity Model surpasses other models in terms of its simplicity and meaningful parameters, which have a physical basis, unlike other models with non-physical parameters.

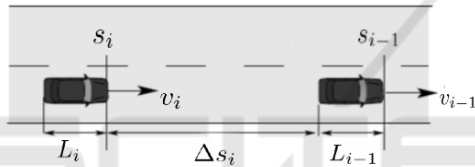


Figure 1: car following notation, image source(Reimann, 2008).

Figure 1 shows two successive vehicles on a road, where s, v, L denote distance progress, velocity, and bumper-to-bumper length of vehicles i and $i-1$.

$$\Delta s_i(t) = s_{i-1}(t) - s_i(t) - L_{i-1} \quad (1)$$

The distance between two vehicles on the road is defined by equation 1. $\Delta s_i(t)$ is also defined as the headway distance $h_i(t)$.

The state variables of the Optimal Velocity Model are headway distance $h_i(t)$ and velocity $v_i(t)$. The Optimal Velocity Model of a vehicle i can be expressed in the form of the following nonlinear equations.

$$\begin{aligned} \dot{h}_i(t) &= v_{i-1}(t) - v_i(t) \\ \dot{v}_i(t) &= F(h_i(t - \tau), \dot{h}_i(t - \tau), v_i(t - \tau)) \end{aligned} \quad (2)$$

Equation 2 indicates that the change in headway of a vehicle is influenced by its velocity and the velocity of the preceding vehicle. It models the acceleration of the vehicle i as a nonlinear function F of the time-shifted headway, the time derivative of the heading, and the vehicle's velocity. The introduced time shift τ is meant to compensate for all incurred delays, with the most significant being the driver's reaction

time. In this work, it is neglected as the system is automated. The nonlinear function F describes the vehicle's velocity state evolution. The definition of F is given in Equation 3.

$$F(h_i, \dot{h}_i, v_i) = \alpha(V(h_i) - v_i) + \beta \dot{h}_i \quad (3)$$

The variables α and β are control gains corresponding to the link between vehicle i and $i-1$. The selection of these parameters is very important and should be carefully studied, taking into consideration the vehicle capabilities. The function V defines the continuous range policy that commands the vehicle velocity and is known as the range policy, defined based on two boundary variables h_{st} the stop headway and h_{go} the free speed headway. They represent the minimum headway distance the vehicle should maintain and the maximum headway distance at which the velocity of the vehicle is v_{max} .

$$V(h) = \begin{cases} 0 & \text{if } h_i \leq h_{st} \\ f_v(h_i) & \text{if } h_{st} < h_i < h_{go} \\ v_{max} & \text{if } h_i \geq h_{go} \end{cases} \quad (4)$$

Indeed, many possible functions can be introduced to achieve an increasing piecewise function; in (Zhang and Orosz, 2013), three candidates of $f_v(h_i)$ were presented.

$$\begin{aligned} f_{v1}(h_i) &= v_{max} \frac{h_i - h_{st}}{h_{go} - h_{st}}, \\ f_{v2}(h_i) &= \frac{v_{max}}{2} \left[1 - \cos \left(\pi \frac{h_i - h_{st}}{h_{go} - h_{st}} \right) \right], \\ f_{v3}(h_i) &= \frac{v_{max}}{2} \left[1 + \tanh \left(\tan \left(\frac{\pi}{2} \frac{2h_i - h_{go} - h_{st}}{h_{go} - h_{st}} \right) \right) \right], \end{aligned} \quad (5)$$

Among these, f_{v1} is not a suitable option since it does not yield a continuous derivative function. Non-smooth transitions occur at h_{st} and h_{go} , leading to discontinuities in the jerk and discomfort for the driver. Therefore, f_{v1} is ruled out. Both f_{v2} and f_{v3} exhibit very similar behaviors. Up to this point, the introduced model incorporates only two vehicles. An enhancement to the model is proposed in (Zhang and Orosz, 2015). They introduce the MOTIF biological concept with some modifications. The concept, used as a vehicle MOTIF m , observes the states of the immediate vehicle ahead, as well as the m -th vehicle ahead. This requires velocity value of the vehicle i , preceding vehicle $i-1$ and the m -th vehicle ahead $i-m$.

It also requires headway value of vehicle's headway h_i , and all headway values of the vehicles from $i-m+1$ to i .

$$\begin{aligned} \dot{h}_i(t) &= v_{i-1}(t) - v_i(t), \\ \dot{v}_i(t) &= \alpha_1 (V(h_i(t)) - v_i(t)) + \beta_1 (v_{i-1}(t) - v_i(t)) + \\ &\quad \alpha_m \left(V \left(\frac{1}{m} \sum_{k=i-m+1}^i h_k(t) \right) - v_i(t) \right) + \\ &\quad \beta_m (v_{i-m}(t) - v_i(t)) \end{aligned} \quad (6)$$

As observed in (6), the velocity of vehicle i relies on the variables v_i , v_{i-1} , v_{i-m} , h_i , and the average of h from the vehicle i to vehicle $i-m+1$. Equation (6) is designated as the optimal velocity model. As previously mentioned, given the non-linear function V defined in (4), the model linearization around a chosen equilibrium point is proceeded.

2.1 Linearization of the Optimal Velocity Model

This section outlines the linearization process of (6). The linearization is performed around a specific point known as an equilibrium point, which characterizes the system dynamics within the vicinity of an operational boundary. This step is imperative for linear control approaches in system analysis and control.

The equilibrium point is represented by h_i^* and v_i^* . The system states h_i, v_i are expressed in relation to the equilibrium point, with the headway defined as $h_i = h_i^* + \tilde{h}_i$ and the velocity as $v_i = v_i^* + \tilde{v}_i$. The tilde symbol signifies the deviation of the vehicle state from the equilibrium point. The first two terms of the Taylor's approximation are considered.

Let's take the first equation from (6) and substitute all variables relative to the operating point.

According to Taylor expansion, any function can be approximated

$$\begin{aligned} f(x) &= f(x^*) + \frac{f'(x^*)}{1!} (x - x^*) + \\ &\quad \frac{f''(x^*)}{2!} (x - x^*)^2 + \frac{f'''(x^*)}{3!} (x - x^*)^3 + \dots, \end{aligned} \quad (7)$$

In order to linearize the system only the first two terms of the equation should be considered. Taking the first state equation from (6), it is rewritten relative to the operating point, resulting in

$$\begin{aligned} \dot{h}_i &= v_{i-1} - v_i \\ \frac{d(h^* + \tilde{h}_i)}{dt} &= v_{i-1}^* + \tilde{v}_{i-1} - v_i^* + \tilde{v}_i \end{aligned} \quad (8)$$

Since h^* and v^* are constant, the equation becomes

$$\dot{\tilde{h}}_i = \tilde{v}_{i-1} - \tilde{v}_i \quad (9)$$

Similarly, the second state v_i is linearized.

$$\begin{aligned} \dot{v}_i &= f(v_{i-1}^*, v_i^*, h_i^*, v_{i-m}^*, h_{i-m+1}^*, h_{i-m+2}^*, \dots, h_{i-1}^*) \\ &\quad + \frac{\partial f(v_{i-1}^*)}{\partial v_{i-1}} (\tilde{v}_i) + \frac{\partial f(v_{i-m}^*)}{\partial v_i} (\tilde{v}_i) + \frac{\partial f(h_i^*)}{\partial h_i} (\tilde{h}_i) \\ &\quad + \frac{\partial f(h_{i-m}^*)}{\partial v_{i-m}} (\tilde{v}_{i-m}) + \frac{\partial f(h_{i-m+1}^*)}{\partial h_{i-m+1}} (\tilde{h}_{i-m+1}) \\ &\quad + \frac{\partial f(h_{i-m+2}^*)}{\partial h_{i-m+2}} (\tilde{h}_{i-m+2}) + \dots + \frac{\partial f(h_i^*)}{\partial h_i} (\tilde{h}_i) \end{aligned} \quad (10)$$

The partial derivatives are given in equation 11.

$$\begin{aligned} \frac{\partial f}{\partial v_{i-1}} &= \beta_1, \quad \frac{\partial f}{\partial v_i} = -\beta_m - \beta_1 - \alpha_1 - \alpha_m \\ \frac{\partial f}{\partial h_i} &= \alpha_1 V'(h_i^*), \quad \frac{\partial f}{\partial v_{i-m}} = \beta_m \\ \frac{\partial f}{\partial h_{i-m+1}} &= \frac{\alpha_m}{m} V'(h_{i-m+1}^*), \\ \frac{\partial f}{\partial h_{i-m+2}} &= \frac{\alpha_m}{m} V'(h_{i-m+2}^*), \dots, \\ \frac{\partial f}{\partial h_i} &= \frac{\alpha_m}{m} V'(h_i^*) \end{aligned} \quad (11)$$

The below equation 12 describes the linearized system.

$$\begin{aligned} \dot{\tilde{h}}_i &= \tilde{v}_{i-1} - \tilde{v}_i \\ \dot{\tilde{v}}_i &= \beta_1 \tilde{v}_{i-1} - (\alpha_1 + \beta_1 + \alpha_m + \beta_m) \tilde{v}_i + \alpha_1 V' \tilde{h}_i + \beta_1 \tilde{v}_{i-m} \\ &\quad + \frac{\alpha_m V' \tilde{h}_i}{m} + \frac{\alpha_m V'}{m} (\tilde{h}_{i-1} + \tilde{h}_{i-2} + \dots + \tilde{h}_{i-m+1}) \end{aligned} \quad (12)$$

The system of linear equations in equation 13 describes the dynamics of the enhanced CACC of MOTIF m when $m > 1$. In the case of $m = 1$, all parameters with m subscript are set to zero. Table 1 lists all numerical values of the OVM parameters used for analytical analysis and numerical simulation.

$$\begin{aligned} \begin{bmatrix} \dot{\tilde{h}}_i \\ \dot{\tilde{v}}_i \end{bmatrix} &= \begin{bmatrix} 0 & & & -1 \\ \alpha_1 V' + \frac{\alpha_m V'}{m} & & -(\alpha_1 + \alpha_m + \beta_1 + \beta_m) & \end{bmatrix} \begin{bmatrix} \tilde{h}_i \\ \tilde{v}_i \end{bmatrix} \\ &\quad + \begin{bmatrix} 1 \\ \beta_1 \end{bmatrix} \tilde{v}_{i-1} + \begin{bmatrix} 0 \\ \beta_m \end{bmatrix} \tilde{v}_{i-m} \\ &\quad + \begin{bmatrix} 0 \\ \frac{\alpha_m V'}{m} \end{bmatrix} \sum_{k=i-m+1}^{i-1} (\tilde{h}_k) + \begin{bmatrix} 0 \\ 1 \end{bmatrix} \tilde{u} \\ \tilde{y} &= \begin{bmatrix} 1 & 0 \end{bmatrix} \begin{bmatrix} \tilde{h}_i \\ \tilde{v}_i \end{bmatrix} \end{aligned} \quad (13)$$

Table 1: Optimal Velocity Model Parameters.

Parameter	Value
α_1	2
α_m	2
β_1	2
β_m	2
V'	$\frac{\pi}{2}$
h_i^*	20 [m]
v_i^*	15 [m/s]
h_{st}	5 [m]
h_{go}	35[m]

2.2 Linearized Model Validity

In this section the accuracy of the linearized model is investigated.

To this end, a simple Cooperative Adaptive Cruise Control (CACC) system consisting of three vehicles is defined. The leading vehicle denoted as $i = 0$, will not be investigated as it is not an Optimal Velocity Model (OVM) vehicle and is modeled as a linear first-order system. The middle vehicle denoted as $i = 1$, is considering only one vehicle ahead i.e it has MOTIF1, and the last vehicle, denoted as $i = 2$, is considering two vehicles ahead i.e it has MOTIF2, as depicted in the figure 2.

A scenario with states far from the linearization point, i.e., h^* and v^* , is defined where the initial states are h_1, h_2 equal to 25[m] and v_1, v_2 equal to 0. The leading vehicle starts moving, and states are compared between both the nonlinear OVM equation (8) and the linearized OVM (12). As shown in the figure 3.

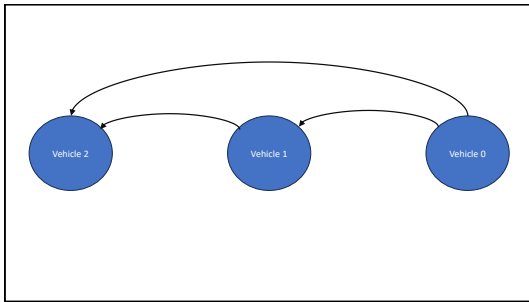


Figure 2: Linearized Model Fidelity Vehicles' Diagram.

To quantify the model validity, the mean squared error is computed. As shown in Figure 3 and Table 2, there is only a minimal deviation between the linearized and non-linear OVM models despite the simulation scenario starting far from the linearization point. This observation suggests that the model is highly faithful.

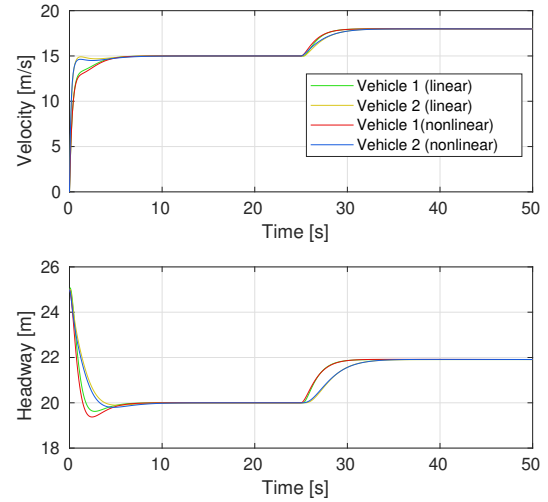


Figure 3: The System States of the Linearized and Nonlinear Model.

Table 2: Mean Squared Error Of The Fidelity Scenario.

State	MSE
v_1	0.0052 [m ² /s ²]
v_2	0.0061 [m ² /s ²]
h_1	0.0124[m ²]
h_2	0.0041[m ²]

3 CONTROLLER DESIGN

The Linear-Quadratic Regulator (LQR) problem is a control problem in which an optimal control law is sought for a linear time-invariant system subject to quadratic cost criteria. The objective is to minimize a quadratic cost function that includes the system's states and control inputs. There are two methods for finding the solution to the linear quadratic regulator problem: Dynamic Programming (Bellman, 1966) and the Pontryagin method (Pontryagin, 1987).

In his dissertation (Nguyen and Bestle, 2007), Nguyen presented a well-documented and complete solution to the linear quadratic regulator problem with disturbances by applying the Pontryagin principle.

3.1 Linear Quadratic Regulator

Here, the problem of the linear quadratic regulator with disturbances is defined and found its solution. Considering a linear time-invariant system with affecting disturbances on the states and measurement model.

$$\begin{aligned} \dot{x} &= \mathbf{A}x + \mathbf{B}u + \mathbf{B}_w w, & x(0) &= x_0 \\ y &= \mathbf{C}x + \mathbf{D}u + \mathbf{D}_w w \end{aligned} \quad (14)$$

where the vectors $x \in \mathbb{R}^n, y \in \mathbb{R}^m, u \in \mathbb{R}^p, w \in \mathbb{R}^q$ represent the states, the measured outputs, the control inputs and the disturbance input respectively. The matrices $\mathbf{A} \in \mathbb{R}^{n \times n}, \mathbf{B} \in \mathbb{R}^{n \times p}, \mathbf{C} \in \mathbb{R}^{m \times n}, \mathbf{D} \in \mathbb{R}^{n \times q}, \mathbf{B}_w \in \mathbb{R}^{n \times w}, \mathbf{D}_w \in \mathbb{R}^{m \times w}$ represent the state, input, output, feed-through, input disturbance, and output disturbance respectively. The objective function defines the importance of each state of our system and the energy used, and the cost is a quadratic function of states x and inputs u .

$$J = \int_0^\infty [y^T Q_y y + u^T R_u u] dt \quad (15)$$

where $\mathbf{Q}_y \succ 0, \mathbf{R}_u \succ 0$ are positive definite matrices the weighting matrices of outputs and inputs, respectively. The linear quadratic regulator aims to find the input value that minimizes the objective function as in equation 16.

$$\begin{aligned} \min \quad & \int_0^\infty [y^T Q_y y + u^T R_u u] dt \\ \text{s.t.} \quad & \dot{x} = \mathbf{A}x + \mathbf{B}u + \mathbf{B}_w w \end{aligned} \quad (16)$$

$$\begin{aligned} J &= \int_0^\infty [(\mathbf{C}x + \mathbf{D}u + \mathbf{D}_w w)^T \mathbf{Q}_y (\mathbf{C}x + \mathbf{D}u + \mathbf{D}_w w) + u^T \mathbf{R}_u u] dt \\ &= \int_0^\infty [(\mathbf{C}x + \mathbf{D}u)^T \mathbf{Q}_y (\mathbf{C}x + \mathbf{D}u) + 2(\mathbf{C}x + \mathbf{D}u)^T \mathbf{Q}_y \mathbf{D}_w w \\ &\quad + w^T \mathbf{D}_w^T \mathbf{Q}_y \mathbf{D}_w w + u^T \mathbf{R}_u u] dt \\ &= \int_0^\infty \left[\underbrace{x^T (\mathbf{C}^T \mathbf{Q}_y \mathbf{C}) x}_{:=Q} + 2x^T \underbrace{(\mathbf{C}^T \mathbf{Q}_y \mathbf{D})}_{:=N} u + u^T \underbrace{(\mathbf{D}^T \mathbf{Q}_y \mathbf{D} + \mathbf{R}_u)}_{:=R} u \right] dt \\ &\quad + \int_0^\infty \left[2x^T \underbrace{(\mathbf{C}^T \mathbf{Q}_y \mathbf{D}_w)}_{:=N_{xw}} w + 2w^T \underbrace{(\mathbf{D}_w^T \mathbf{Q}_y \mathbf{D})}_{:=N_{wv}} u + w^T \underbrace{(\mathbf{D}_w^T \mathbf{Q}_y \mathbf{D}_w)}_{:=R_w} w \right] dt \\ &= \int_0^\infty \left[x^T \mathbf{Q} x + 2x^T \mathbf{N} u + u^T \mathbf{R} u \right] dt + \int_0^\infty \left[2x^T \mathbf{N}_{xw} w + 2w^T \mathbf{N}_{wv} u + w^T \mathbf{R}_w w \right] dt \\ &=: \int_0^\infty \mathcal{F}(u, x, w, t) dt \end{aligned} \quad (17)$$

The equation (16) shows the complete definition of LQR problem as an optimization problem. The solution to this problem is mathematically not straight forward, as stated before. The solution is shown. Substituting the y in the equation (16)

The control law is composed of two parts: the state feedback term, which relates the input to the state vector x , and the disturbance feed-forward term, which relates the input to the disturbance vector w :

$$\mathbf{u} = u_x + u_w = \mathbf{K}_x x + \mathbf{K}_w w \quad (18)$$

The equation (19) represents the formula for the state feedback gain \mathbf{K}_x , while the disturbance feed-forward gain \mathbf{K}_w is shown in (20).

$$\mathbf{K}_x = -\mathbf{R}^{-1} (\mathbf{N}^T + \mathbf{B}^T \mathbf{P}) \quad (19)$$

$$\mathbf{K}_w = -\mathbf{R}^{-1} \left(\mathbf{N}_{wv}^T + \mathbf{B}^T [\mathbf{A}^T + (\mathbf{K}_x)^T \mathbf{B}^T]^{-1} [(\mathbf{K}_x)^T \mathbf{N}_{wv}^T - (\mathbf{N}_{xw} + \mathbf{P} \mathbf{B}_w)] \right) \quad (20)$$

The matrix \mathbf{P} , which appears in both formulas for \mathbf{K}_x and \mathbf{K}_w , is known as the Riccati matrix. The value of \mathbf{P} satisfies the equality 21. Further details can be found in (Naidu, 2002), page 129.

$$\mathbf{P} \mathbf{A} + \mathbf{A}^T \mathbf{P} - (\mathbf{P} \mathbf{B} + \mathbf{N}) \mathbf{R}^{-1} (\mathbf{N}^T + \mathbf{B}^T \mathbf{P}) + \mathbf{Q} = \mathbf{0} \quad (21)$$

Upon revisiting the state space model in the equation (13), where \mathbf{D} and \mathbf{D}_w are zero, all non- $(\tilde{h}_i, \tilde{v}_i, \tilde{u})$ can be lumped into the disturbance matrix \mathbf{B}_w . Consequently, the control gains \mathbf{K}_x and \mathbf{K}_w take the form:

$$\mathbf{K}_x = -\mathbf{R}^{-1} (\mathbf{B}^T \mathbf{P}) \quad (22)$$

$$\mathbf{K}_w = -\mathbf{R}^{-1} \left(\mathbf{B}^T [\mathbf{A}^T + (\mathbf{K}_x)^T \mathbf{B}^T]^{-1} (\mathbf{P} \mathbf{B}_w) \right) \quad (23)$$

Several key points regarding the obtained control formula are discussed in this section.

- The optimal feed-forward disturbance gain \mathbf{K}_w , as shown in formula 23, depends not only on the system definition and the assigned input cost matrix but also on the optimal state feedback gain \mathbf{K}_x .
- By setting \mathbf{K}_w to zero, the result of an LQR is obtained. In this case, the control formula does not compensate for the measured disturbances w , but the control is still able to keep the states still, albeit more slowly than when \mathbf{K}_w is incorporated.
- LQR does not consider the physical limits of the system, such as saturation, making the selection of the weighting matrices \mathbf{R} and \mathbf{Q} challenging. Extensive simulations are necessary to ensure that the controller does not push the system to its actuation limits. Other controllers, such as MPC and the constrained LQR (Sokaert and Rawlings, 1998), perform better in this aspect.
- LQR maintains the system at a specific state when the reference signal is 0. If the reference signal changes or disturbances occur, a steady-state error appears. To make the system follow the reference input, either adding a state to the system to represent the error between the reference signal and the output, known as state augmentation (Åström and Murray, 2021), or incorporating the system's disturbances, known as optimal disturbance feed-forward with the gain matrix \mathbf{K}_w .
- The state augmentation process makes the selection of \mathbf{R} and \mathbf{Q} even more difficult because the additional system state has a linear relationship with the other states.
- Alternatively, the LQR can be used to solve the regulating problem, whereas a manually tuned

gain is used to eradicate the steady-state error. However, this means the controller is optimal in regulating the states but not necessarily in tracking the input reference.

All controllers have been designed with the system values as per table 1 for MOTIF1. For other MOTIF configurations, the values are $\alpha_1 = 1.5$, $\alpha_m = 1$, $\beta_1 = 0.6$, and $\beta_m = 0.9$. This modification makes the system matrix A for all MOTIF configurations identical. This makes one controller universal for any MOTIF and allows us to inspect the impact of the MOTIF configuration on the whole system as well as the controller performance.

Before finding the control gains of the state-space model in (13), the controllability needs to be checked. The controllability matrix $C = [B, AB]$ should be a full-rank matrix.

$$\begin{bmatrix} 0 & -1 \\ 1 & -\alpha_1 - \alpha_m - \beta_1 - \beta_m \end{bmatrix} \quad (24)$$

The system in (13) has a full-rank controllability matrix (24). Designing an LQR controller for the system described in (13) does not yield zero steady-state error. The controller maintains the system at a specific state when the system is at its linearization point. However, when the leading or preceding vehicle changes its velocity, the following vehicle deviates from the linearization point, and a steady-state error appears. This happens because the controller does not account for the other signals, i.e., $\tilde{v}_{i-1}, \tilde{v}_{i-m}, \dots$. The selection of the weighting matrices is an iterative process where satisfactory system response is obtained. The control gains can be found using MATLABTM's `lqr` function with the weighting matrices \mathbf{Q} and \mathbf{R} . The control gain matrix \mathbf{K}_x .

$$\mathbf{K}_x = - \begin{bmatrix} -16.7064 & 3.0365 \end{bmatrix} \quad (25)$$

The Riccati matrix \mathbf{P} .

$$\mathbf{P} = \begin{bmatrix} 123.5829 & -16.7064 \\ -16.7064 & 3.0365 \end{bmatrix} \quad (26)$$

3.2 Linear Quadratic Regulator with Disturbance Feed-Forward

Simulations show that the Linear Quadratic Regulator does not yield zero steady-state error. In this section, the LQR with a disturbance feed-forward term is combined. By substituting the \mathbf{K}_x equation (25) and the \mathbf{P} equation (23) in equation (23), the gain $\mathbf{K}_w = 6.64$ which is valid only for MOTIF1.

Simulation of this controller shows that it was able to reach a zero steady-state error. Tuning of the disturbance gain \mathbf{K}_w is not possible because it depends

on \mathbf{K}_x . A small change in \mathbf{K}_w makes the controller not valid in that particular case, and steady-state error appears. One last caveat is that this controller allows the disturbance signals to propagate and be amplified through the following vehicles even with a low \mathbf{K}_w value.

3.3 Linear Quadratic Regulator with Integral Action

To ensure that the controller precisely follows the reference input, the second approach is to incorporate integral action. This involves introducing an additional state to represent the error between the reference signal and the output a process known as Integral action (Malkapure and Chidambaram, 2014). The new state is defined as $\dot{\tilde{e}}_i = \tilde{r}_i - \tilde{h}_i$, where \tilde{r}_i is the desired headway reference. This new state equation is added to the state space equation (13).

$$\begin{bmatrix} \dot{\tilde{h}}_i \\ \dot{\tilde{v}}_i \\ \dot{\tilde{e}}_i \end{bmatrix} = \begin{bmatrix} 0 & -1 & 0 \\ \alpha_1 V' + \frac{\alpha_m V'}{m} & -(\alpha_1 + \alpha_m + \beta_1 + \beta_m) & 0 \\ -1 & 0 & 0 \end{bmatrix} \begin{bmatrix} \tilde{h}_i \\ \tilde{v}_i \\ \tilde{e}_i \end{bmatrix} + \begin{bmatrix} 0 \\ 1 \\ 0 \end{bmatrix} \tilde{u}_i + \begin{bmatrix} 1 \\ \beta_1 \\ 0 \end{bmatrix} \tilde{v}_{i-1} + \begin{bmatrix} 0 \\ \beta_m \\ 0 \end{bmatrix} \tilde{v}_{i-m} + \begin{bmatrix} 0 & \frac{\alpha_m V'}{m} \\ 0 & 0 \end{bmatrix} \sum_{k=i-m+1}^{i-1} (\tilde{h}_k) + \begin{bmatrix} 0 \\ 0 \\ 1 \end{bmatrix} \tilde{r}_i$$

$$\dot{\tilde{y}} = \begin{bmatrix} 1 & 0 & 0 \end{bmatrix} \begin{bmatrix} \tilde{h}_i \\ \tilde{v}_i \\ \tilde{e}_i \end{bmatrix} \quad (27)$$

The controllability matrix $C = [B, AB, A^2B]$ in (28) is a full rank matrix.

$$\begin{bmatrix} 0 & -1 & \alpha_1 + \alpha_m + \beta_1 + \beta_m \\ 1 & -\alpha_1 - \alpha_m - \beta_1 - \beta_m & (\alpha_1 + \alpha_m + \beta_1 + \beta_m)^2 - V' \alpha_1 - \frac{V' \alpha_m}{m} \\ 0 & 0 & 1 \end{bmatrix} \quad (28)$$

Using the same weighting matrices as per subsection 3.1 controller with an additional row to account for the weight of the new state. The following control gain matrix is obtained \mathbf{K}_x

$$\mathbf{K}_x = - \begin{bmatrix} -16.7064 & 3.0365 & 1.0000 \end{bmatrix} \quad (29)$$

The simulation results show that this controller is able to achieve zero steady-state error. The integral action term of the control formula is easily tuned and decoupled from other states' gains. This controller shows wave propagation through the following vehicles. However, it is not as severe as with the controller in section 3.2.

4 CLOSED LOOP SIMULATION

In this section, two simulation scenarios are presented. The first scenario involves a leading vehicle

changing velocity. The focus is on MOTIF1, MOTIF2, and MOTIFn. MOTIF1 and MOTIF2 are considered fundamentals and MOTIFn is for the purpose of studying the direct signal propagation throughout the vehicles.

The second simulation scenario involves the injection of a disturbance in a vehicle's velocity. The focus is on MOTIF1 and MOTIF2. The behavior of the vehicle and the following vehicles behind the disturbed vehicle are inspected.

The control law is derived as feedback gains in Equation (29).

4.1 Leading Vehicle Changing Velocity Scenario

Several vehicles are set up, with the leading vehicle $i = 0$ accelerating from 15 m/s to 18 m/s instantly. This scenario mimics a step-input disturbance to the following vehicles. The controller should adapt to the new velocity and drive back the distance headway to its desired level, i.e., 20 m.

4.1.1 MOTIF1 Closed-Loop Simulation

In this simulation scenario, the first vehicle is modeled as a step-input signal. All other vehicles are modeled using MOTIF1. Therefore, they only take into account the vehicle directly ahead. The vehicles can follow the desired speed defined by the leading vehicle. At the same time, the controller drives the headway distance to its desired level. In this MOTIF configuration, the vehicle starts compensating for the deviation in states only when the preceding vehicle starts responding.

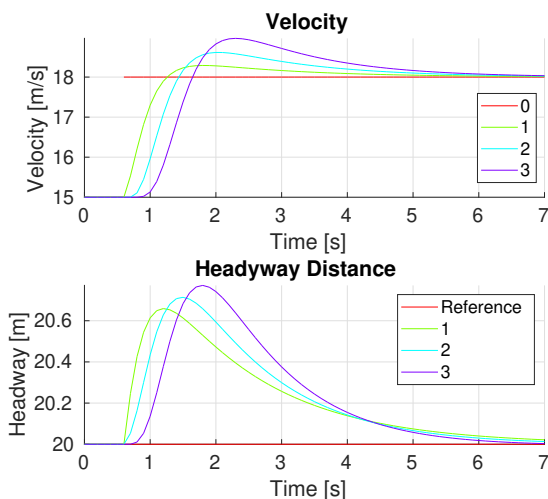


Figure 4: MOTIF1 closed loop simulation of leading vehicle changing velocity scenario.

4.1.2 MOTIF2 Closed Loop Simulation

In this simulation scenario, five vehicles exist. The first vehicle is modeled as a step-input signal. The second vehicle is modeled using OVM with MOTIF1 since MOTIF2 is not defined for it. The rest of the vehicles are modeled using the optimal velocity model of MOTIF2. The steady state of this configuration is identical to Section 4.1.1. However, the transient response takes place earlier as per the imposed MOTIF configuration. Higher velocity overshoots are observed and less headway distance overshoots than in Section 4.1.1.

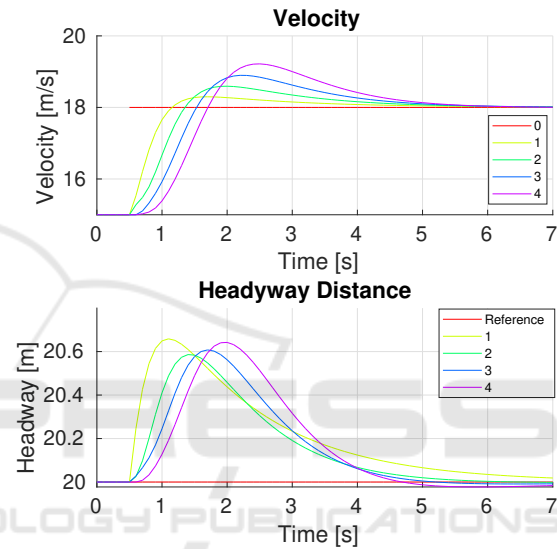


Figure 5: MOTIF2 closed loop simulation of leading vehicle changing velocity scenario.

4.1.3 MOTIFn Closed Loop Simulation

In this simulation scenario, 5 vehicles are instantiated. Each vehicle's MOTIF equals its i subscript; for example, the vehicle with $i = 1$ is MOTIF1, and the vehicle with $i = 2$ is MOTIF2, and so on. This configuration allows each vehicle to obtain the velocity of each preceding and leading vehicle. In Figure 6, the vehicles start responding by increasing their velocities at the exact time point when the leading vehicle changes its velocity. This MOTIF configuration has the highest overshoot in both velocity and headway, this happens because the controller does not discriminate between disturbance signals i.e. \tilde{v}_{i-1} and \tilde{v}_{i-m} and the integral gains are the same for all vehicles. More careful selection of the integral gain reduces the overshoot.

In the MOTIFn configuration, the responsiveness for perpetuation is simultaneous in which the follow-

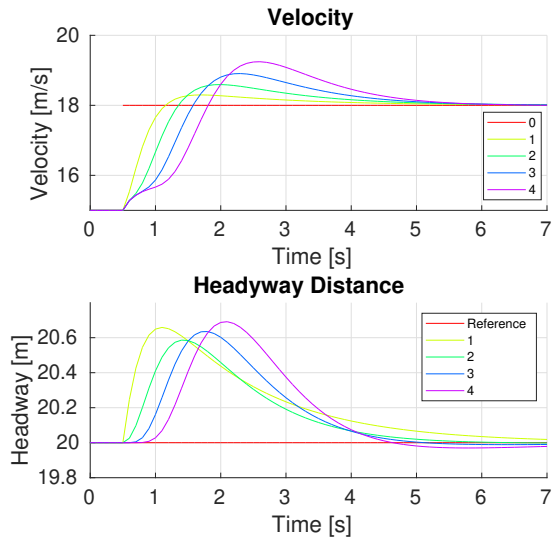


Figure 6: MOTIFn closed loop simulation of leading vehicle changing velocity scenario.

ing vehicles start responding at the time instance of perpetuation occurring which is a significant advantage over other CACC systems where they respond asynchronously as in (Bekiaris-Liberis, 2023), (Chen et al., 2024) (Xing et al., 2022) and others. By implementing a comprehensive assessment mechanism, we can pinpoint and address the vulnerabilities in our CACC. This targeted approach will enable us to enhance the overall resilience and responsiveness of our transportation system by making vulnerable vehicle central in the information flow and the other vehicles respond to the vulnerable vehicles simultaneously.

In all simulation scenarios of different MOTIFs, the controller is able to keep the desired headway even when the dynamics are different.

4.2 Velocity Disturbance Scenario

Several vehicles are set up, a non-leading vehicle velocity is injected with a velocity disturbance. This allows us to inspect the controller on the vehicle level and on the following vehicles. This scenario mimics an impulse input to the vehicle and an impulse disturbance on the following vehicles.

4.2.1 MOTIF1 Closed Loop Simulation

Figure 7 shows the states' evolution of three MOTIF1 vehicles. An impulse occurs in vehicle 1. The vehicle states return to the desired state with an overshoot in the headway value. The following vehicles also return to the desired states.

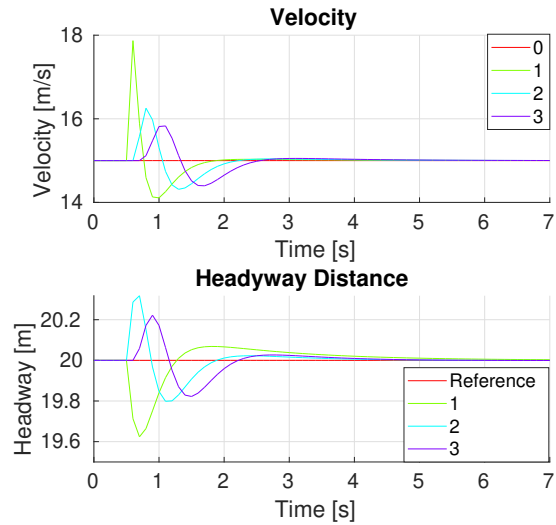


Figure 7: MOTIF1 closed loop simulation of leading vehicle 1 velocity disturbance scenario.

4.2.2 MOTIF2 Closed Loop Simulation

In this simulation, vehicle 1 is MOTIF1, and the following vehicles are MOTIF2. An impulse occurs in vehicle 2. The vehicle returns to the desired state. 8. The following vehicles of vehicle 2 start responding to impulse at the same time.

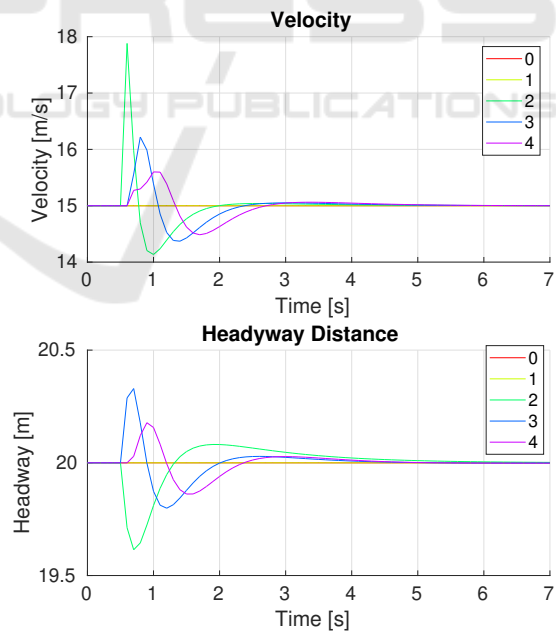


Figure 8: MOTIF2 closed loop simulation of leading vehicle changing velocity scenario.

In both cases subsections 4.2.1 and 4.2.2 the controller deals with the disturbance without showing signal propagation in either velocity or headway from leading to following vehicles.

5 CONCLUSION

In this work, a new CACC system that exhibits the Optimal Velocity Model has been introduced. The new CACC system uses the adopted MOTIF concept to define the system dynamics. The linearized dynamic equations have been derived for any MOTIF. Several Linear Quadratic Controllers have been included. The main focus was on LQR with integral action. Simulations of different MOTIFs were presented. The LQR with the integral action controller is able to bring the system states to the desired value and is indifferent to the MOTIF. In this work, the internal dynamics of the vehicles were ignored. Inclusion of longitudinal dynamics as a first-order linear system is a potential future work. From an vehicle perspective, the LQR with integral action performs very well; however, from a multiple-vehicles perspective, it is clear that wave propagation through vehicles takes place, this happens as a result of the integral part of the controller. This limitation is very significant and needs to be addressed in further future work.

REFERENCES

- Åström, K. J. and Murray, R. M. (2021). *Feedback systems: an introduction for scientists and engineers*. Princeton university press.
- Bando, M., Hasebe, K., Nakayama, A., Shibata, A., and Sugiyama, Y. (1994). Structure stability of congestion in traffic dynamics. *Japan Journal of Industrial and Applied Mathematics*, 11(2):203–223.
- Bando, M., Hasebe, K., Nakayama, A., Shibata, A., and Sugiyama, Y. (1995). Dynamical model of traffic congestion and numerical simulation. *Physical review E*, 51(2):1035.
- Bekiaris-Liberis, N. (2023). Robust String Stability and Safety of CTH Predictor-Feedback CACC. *IEEE Trans. Intell. Transp. Syst.*, 24(8):8209–8221.
- Bellman, R. (1966). Dynamic programming. *Science*, 153(3731):34–37.
- Brand, C., Anable, J., and Morton, C. (2019). Lifestyle, efficiency and limits: modelling transport energy and emissions using a socio-technical approach. *Energy Efficiency*, 12(1):187–207.
- Chen, D., Zhang, K., Wang, Y., Yin, X., Li, Z., and Filev, D. (2024). Communication-efficient decentralized multi-agent reinforcement learning for cooperative adaptive cruise control. *IEEE Transactions on Intelligent Vehicles*.
- Fu, A., Chen, S., Qiao, J., and Yu, C. (2023). Periodic Event-Triggered CACC and Communication Co-design for Vehicle Platooning. *ACM Trans. Cyber-Phys. Syst.*, 7(4):1–19.
- Ge, J. I. and Orosz, G. (2016). Optimal Control of Connected Vehicle Systems With Communication Delay and Driver Reaction Time. *IEEE Trans. Intell. Transp. Syst.*, 18(8):2056–2070.
- Hsueh, K.-F., Farnood, A., Al-Darabsah, I., Al Saaideh, M., Al Janaideh, M., and Kundur, D. (2022). A Deep Time Delay Filter for Cooperative Adaptive Cruise Control. *ACM Trans. Cyber-Phys. Syst.*
- Liu, J., Zhou, Y., and Liu, L. (2023). Communication delay-aware cooperative adaptive cruise control with dynamic network topologies—a convergence of communication and control. *Digital Communications and Networks*.
- Malkapure, H. G. and Chidambaram, M. (2014). Comparison of two methods of incorporating an integral action in linear quadratic regulator. *IFAC Proceedings Volumes*, 47(1):55–61.
- Naidu, D. S. (2002). *Optimal control systems*. CRC press.
- Nguyen, T.-A. and Bestle, D. (2007). Application of optimization methods to controller design for active suspensions. *Mechanics based design of structures and machines*, 35(3):291–318.
- Pontryagin, L. S. (1987). *Mathematical theory of optimal processes*. CRC press.
- Reimann, M. (2008). Simulationsmodelle im Verkehr. <https://docplayer.org/39907139-Simulationsmodelle-im-verkehr.html>. [Online; Sep, 2022].
- Scokaert, P. O. and Rawlings, J. B. (1998). Constrained linear quadratic regulation. *IEEE Transactions on automatic control*, 43(8):1163–1169.
- Shladover, S. E., Nowakowski, C., Lu, X.-Y., and Ferlis, R. (2015). Cooperative adaptive cruise control: Definitions and operating concepts. *Transportation Research Record*, 2489(1):145–152.
- Wang, Z., Wu, G., and Barth, M. J. A Review on Cooperative Adaptive Cruise Control (CACC) Systems: Architectures, Controls, and Applications. In *2018 21st International Conference on Intelligent Transportation Systems (ITSC)*, pages 04–07. IEEE.
- Xing, H., Ploeg, J., and Nijmeijer, H. (2022). Robust CACC in the Presence of Uncertain Delays. *IEEE Trans. Veh. Technol.*, 71(4):3507–3518.
- Yang, T., Murguia, C., Nešić, D., and Lv, C. (2023). A Robust CACC Scheme Against Cyberattacks via Multiple Vehicle-to-Vehicle Networks. *IEEE Trans. Veh. Technol.*, 72(9):11184–11195.
- Zhang, L. and Orosz, G. (2013). Designing network motifs in connected vehicle systems: delay effects and stability. In *Dynamic Systems and Control Conference*, volume 56147, page V003T42A006. American Society of Mechanical Engineers.
- Zhang, L. and Orosz, G. (2015). Connected vehicle systems with nonlinear dynamics and time delays. *IFAC-PapersOnLine*, 48(12):370–375.
- Zhongwei, F., Qin, K., Jiao, X., Du, F., and Li, D. Cooperative Adaptive Cruise Control for Vehicles Under False Data Injection Attacks. In *2023 IEEE 6th International Conference on Industrial Cyber-Physical Systems (ICPS)*, pages 08–11. IEEE.